Fractional Quantum Hall Effect of Hard-Core Bosons in Topological Flat Bands

Yi-Fei Wang, Zheng-Cheng Gu, Chang-De Gong, and D. N. Sheng

Phys. Rev. Lett. **107**, 146803 — Published 30 September 2011

DOI: 10.1103/PhysRevLett.107.146803

Fractional Quantum Hall Effect of Hard-Core Bosons in Topological Flat Bands

Yi-Fei Wang[1,2], Zheng-Cheng Gu[3], Chang-De Gong[1,4], and D. N. Sheng[2]

[1]*Center for Statistical and Theoretical Condensed Matter Physics, and Department of Physics, Zhejiang Normal University, Jinhua 321004, China*

[2]*Department of Physics and Astronomy, California State University, Northridge, California 91330, USA*

[3]*Kavli Institute for Theoretical Physics, University of California, Santa Barbara, California 93106, USA*

[4]*National Laboratory of Solid State Microstructures and Department of Physics, Nanjing University, Nanjing 210093, China*

Abstract

Recent proposals of topological flat band (TFB) models have provided a new route to realize the fractional quantum Hall effect (FQHE) without Landau levels. We study hard-core bosons with short-range interactions in two representative TFB models, one of which is the well-known Haldane model (but with different parameters). We demonstrate that FQHE states emerge with signatures of even number of quasi-degenerate ground states on a torus and a robust spectrum gap separating these states from higher energy spectrum. We also establish quantum phase diagrams for the filling factor 1/2 and illustrate quantum phase transitions to other competing symmetry-breaking phases.

PACS numbers: 73.43.Cd, 05.30.Jp, 71.10.Fd, 37.10.Jk

Introduction.—The fractional quantum Hall effect (FQHE), one of the most fascinating discoveries in two-dimensional (2D) electron gas, has set up a paradigm to explore new topological phases in other strongly correlated systems. As commonly believed, the FQHE requires two basic ingredients: single-particle states with nontrivial topology, and quenching of the kinetic energy compared to interaction energy scale. However, despite of the seemingly universal theoretical concepts, the FQHE has only been found in 2D systems under a strong perpendicular magnetic field, i.e., in which particles move in Landau levels (LLs). In rotating Bose-Einstein condensate [1] and optical lattice systems [2, 3], researchers have been interested in generating an artificial uniform magnetic field, thus the bosonic FQHE states are expected, but still due to the existence of LLs.

Haldane's honeycomb lattice model [4] and other similar lattice models [5, 6] have two nontrivial topological bands characterized by ± 1 Chern numbers [7, 8], demonstrating the integer quantum Hall effect without LLs. However, these single-particle bands are still highly dispersive, thus it is unlikely to realize the FQHE in such systems. Recently, proposals of topological flat bands (TFB) [9–11] shed new light on this long-standing and hard problem. These TFB models belong to the same topological class as the Haldane model and are distinct from other flat bands with a zero Chern number [12]. A series of TFB models have been explicitly constructed with a flatness ratio (the ratio of the band gap over bandwidth) reaching a high value between $20 \sim 50$ [9, 11]. A systematic numerical study found both the fermionic 1/3 and 1/5 FQHE of interacting fermions on the checkerboard TFB model [13] (see also Ref. [10]).

We address the possible bosonic FQHE in TFB models filled with interacting hard-core bosons, since the TFB will be more likely realized in optical lattices by manipulating bosonic cold atoms [14–16]. There is an interesting proposal lately to find such bosonic FQHE in frustrated kagomé-lattice magnets [17], in terms of the long-sought chiral spin states [18]. Although TFB models possess both ingredients to realize the FQHE, quantum phases in such systems are determined by some competing effects, different from a LL problem. The main effects are: i) the lattice effect and the residual kinetic energy since a TFB is not strictly flat; ii) the Berry curvature of a TFB has substantial momentum dependence representing a non-uniform magnetic field effect in momentum space; iii) lattice symmetry breaking may lead to other conventional ordered states for hard-core bosons.

In this letter, we present the exact diagonalization (ED) calculations of two represen-

tative TFB models with the nearest-neighbor (NN) and the next-nearest-neighbor (NNN) repulsions V_1 and V_2. We find convincing numerical evidences of both the 1/2 and the 1/4 bosonic FQHE phases which are characterized by the formation of quasi-degenerate ground-state manifold (GSM) with even number of states. The GSM carries a unit total Chern number [19], which is a robust property of the system protected by a finite energy spectrum gap. We also determine phase diagrams for our systems and illustrate the quantum phase transitions based on the calculations of the density structure factors and the fidelity [20] of the ground state (GS) wavefunction.

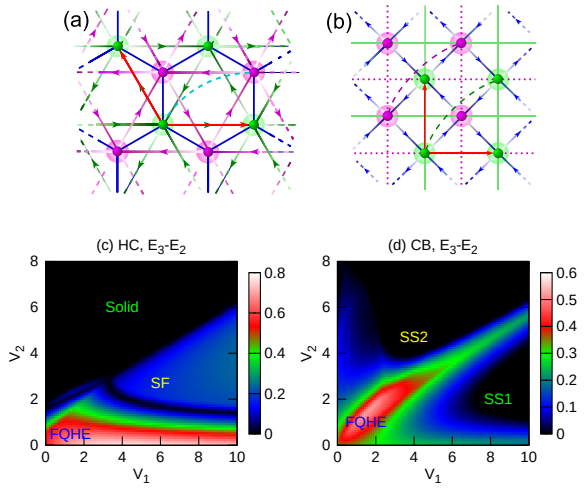

FIG. 1: (color online). (a) The Haldane model on the honeycomb lattice and (b) the checkerboard model. The arrow directions present the signs of the phases $\pm\phi$ in the NNN or NN hopping terms. For the checkerboard lattice, the NNN hopping amplitudes are t' $(-t')$ along the solid (dotted) lines. The NNNN hoppings are represented by the dashed curves in both models. (c)-(d) Intensity plots of spectrum gaps in the V_1-V_2 phase space at $\nu = 1/2$ for (c) 24-site honeycomb lattice; (d) 24-site checkerboard lattice. FQHE, SF, SS1/SS2, and Solid label estimated phase regions inferred from the spectrum-gap plots and other information (see text).

Model Hamiltonians.—The first model is the Haldane model [4] on the honeycomb (HC) lattice filled with interacting hard-core bosons [21]:

$$\begin{aligned} H_{\rm HC} &= -t' \sum_{\langle\langle \mathbf{r}\mathbf{r}'\rangle\rangle} \left[b^\dagger_{\mathbf{r}'} b_{\mathbf{r}} \exp\left(i\phi_{\mathbf{r}'\mathbf{r}}\right) + \text{H.c.} \right] \\ &- t \sum_{\langle \mathbf{r}\mathbf{r}'\rangle} \left[b^\dagger_{\mathbf{r}'} b_{\mathbf{r}} + \text{H.c.} \right] - t'' \sum_{\langle\langle\langle \mathbf{r}\mathbf{r}'\rangle\rangle\rangle} \left[b^\dagger_{\mathbf{r}'} b_{\mathbf{r}} + \text{H.c.} \right] \\ &+ V_1 \sum_{\langle \mathbf{r}\mathbf{r}'\rangle} n_{\mathbf{r}} n_{\mathbf{r}'} + V_2 \sum_{\langle\langle \mathbf{r}\mathbf{r}'\rangle\rangle} n_{\mathbf{r}} n_{\mathbf{r}'} \end{aligned} \tag{1}$$

where $b^\dagger_{\mathbf{r}}$ creates a hard-core boson at site $\mathbf{r}$, $n_{\mathbf{r}}$ is the boson number operator, $\langle \dots \rangle$, $\langle\langle \dots \rangle\rangle$ and $\langle\langle\langle \dots \rangle\rangle\rangle$ denote the NN, the NNN and the next-next-nearest-neighbor (NNNN) pairs of sites, respectively [Fig. 1(a)]. We call this model as a Haldane-Bose-Hubbard (HBH) model [21].

The second model is a variant version of the HBH model on the 2D checkerboard (CB) lattice [5, 11, 22, 23]:

$$\begin{aligned} H_{\rm CB} &= -t \sum_{\langle \mathbf{r}\mathbf{r}' \rangle} \left[b^\dagger_{\mathbf{r}'} b_{\mathbf{r}} \exp\left(i\phi_{\mathbf{r}'\mathbf{r}}\right) + \text{H.c.} \right] \\ &\pm t' \sum_{\langle\langle \mathbf{r}\mathbf{r}' \rangle\rangle} \left[b^\dagger_{\mathbf{r}'} b_{\mathbf{r}} + \text{H.c.} \right] - t'' \sum_{\langle\langle\langle \mathbf{r}\mathbf{r}' \rangle\rangle\rangle} \left[b^\dagger_{\mathbf{r}'} b_{\mathbf{r}} + \text{H.c.} \right] \\ &+ V_1 \sum_{\langle \mathbf{r}\mathbf{r}' \rangle} n_{\mathbf{r}} n_{\mathbf{r}'} + V_2 \sum_{\langle\langle \mathbf{r}\mathbf{r}' \rangle\rangle} n_{\mathbf{r}} n_{\mathbf{r}'} \end{aligned} \tag{2}$$

In the ED study, we consider a finite system of $N_1 \times N_2$ unit cells (total number of sites $N_s = 2 \times N_1 \times N_2$) with basis vectors shown in Figs. 1(a)-(b) and periodic boundary conditions (PBC), implementing translational symmetries and thus the Hilbert space dimension is reduced by a factor about $1/(N_1 N_2)$ [24]. We denote the number of bosons as N_b, and the filling factor of the TFB is thus $\nu = N_b/(N_1 N_2)$. In both models, the amplitude of NN hopping $|t|$ is set as the unit of energy.

Topological flat bands.—On the honeycomb lattice, if we restrict the model with only NN and NNN hoppings, the best TFB has a flatness ratio 7 [10]. By allowing the NNNN hoppings, we numerically found a large class of much flatter bands with nonzero Chern numbers, e.g. a flatness ratio about 50 for the set of parameters, which will be used here: $t = 1$, $t' = 0.60$, $t'' = -0.58$ and $\phi = 0.4\pi$. Using these parameters, the lower TFB is gaped from upper quadratic dispersive band by breaking the time reversal symmetry but preserving other lattice symmetries [11, 23].

On the checkerboard lattice, we adopt the parameters of Ref. [11] with an additional minus sign (to make the TFB as the lower energy band), $t = -1$, $t' = 1/(2+\sqrt{2})$, $t'' = -1/(2+2\sqrt{2})$ and $\phi = \pi/4$, which leads to a TFB with the flatness ratio about 30.

The $\nu = 1/2$ phase diagrams.—We first glance at the spectrum gaps of the two 24-site ($2 \times 4 \times 3$) lattices at the filling $\nu = 1/2$ as shown in Fig. 1(c) and 1(d). E_1, E_2 and E_3 denote the energies of the three lowest eigenstates. For the $\nu = 1/2$ FQHE phase at the left bottom corners in the V_1-V_2 space, there is a GSM with two quasi-degenerate lowest eigenstates, and

the GSM is separated from higher eigenstates by a finite spectrum gap $E_3 - E_2$ ($\gg E_2 - E_1$). The other rough phase regions for the possible superfluid (SF), the supersolids (SS1/SS2) and the solid will be discussed later. We have also obtained numerical results from larger lattice sizes of 32 ($2 \times 4 \times 4$), 36 ($2 \times 6 \times 3$) and 40 ($2 \times 4 \times 5$) sites, and have confirmed both phase diagrams are qualitatively correct.

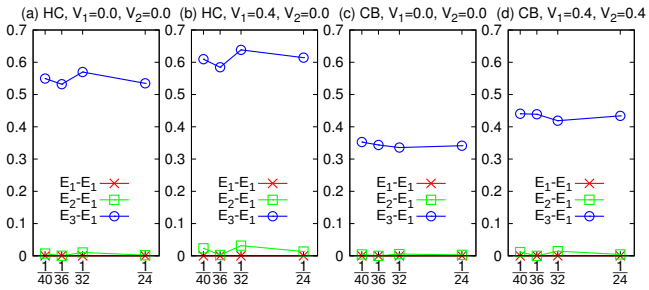

FIG. 2: (color online). 1/2-FQHE spectrum gaps versus $1/N_s$: (a)-(b) honeycomb lattice; (c)-(d) checkerboard lattice.

Low energy spectrum and robust spectrum gap.—We denote the momentum vector $\mathbf{q} = (2\pi k_1/N_1, 2\pi k_2/N_2)$ with (k_1, k_2) as integer quantum numbers. The GSM is defined as a set of lowest states separated from other excited states by a finite spectrum gap. If (k_1, k_2) is the momentum sector for one of the states in the GSM, we find that the other state should be obtained in the sector $(k_1 + N_b, k_2 + N_b)$ [module (N_1, N_2)] . For $N_s = 24$, 36 and 40, the two states within the GSM of a $\nu = 1/2$ FQHE phase are indeed in different momentum sectors: $(0, 0)$ and $(2, 0)$ for $N_s = 24$ and $N_s = 40$, while $(0, 0)$ and $(3, 0)$ for $N_s = 36$. For $N_s = 32$, both N_b/N_1 and N_b/N_2 are integers, thus both states within the GSM are in the $(0, 0)$ sector.

Now we check whether the spectrum gap $E_3 - E_2$ remains in the thermodynamic limit. As shown in Fig. 2, when N_s increases, the spectrum gap $E_3 - E_2$ does not decrease, which extrapolates to a finite value at large N_s limit. Interestingly, the spectrum gap $E_3 - E_2$ is already quite large ($E_3 - E_2 \gg E_2 - E_1$) for hard-core boson system without additional interactions (V_1=V_2=0) [in Figs. 2(a) and 2(c)] demonstrating the robust 1/2 FQHE. The spectrum gap can be slightly enhanced with a small V_1 and/or V_2 [Figs. 2(b) and 2(d)].

By comparing the spectrum gap $E_3 - E_2$ between two lattices for the $V_1 = V_2 = 0.0$ cases in Figs. 2(a) and 2(c), we notice that the gap $E_3 - E_2$ in the honeycomb lattice is obviously larger, which might be due to its larger flatness ratio. After studies on a few more cases

with smaller flatness ratios 7 [10] and 30 (with $t' = 0.40$, $t'' = -0.33$ and $\phi = 0.5\pi$) on the honeycomb lattice, we conclude that the flatter the TFB is, the larger the spectrum gap $E_3 - E_2$ can be, indicating a more robust FQHE, although the global structure of the phase diagram does not change much.

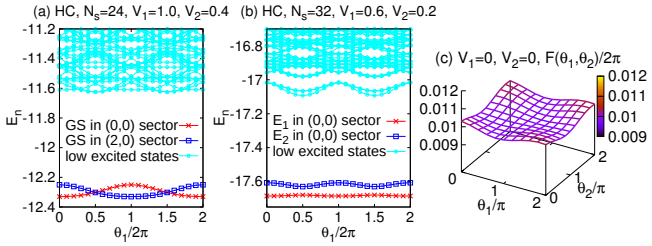

FIG. 3: (color online). (a)-(b) Low energy spectra versus θ_1 at a fixed $\theta_2 = 0$ for two honeycomb lattices at $\nu = 1/2$. (c) $F(\theta_1, \theta_2)\Delta\theta_1\Delta\theta_2/2\pi$ at 10×10 mesh points for a GSM of the 32-site honeycomb lattice.

Berry curvature and Chern number.—Introducing two boundary phases θ_1 and θ_2 as the generalized boundary conditions in both directions, the Chern number [7] (is also the Berry phase in units of 2π) of a many-body state is given by an integral in the boundary phase space [8, 19]: $C = \frac{1}{2\pi}\int\int d\theta_1\theta_2 F(\theta_1, \theta_2)$, where the Berry curvature is given by $F(\theta_1, \theta_2) = \mathrm{Im}\left(\left\langle \frac{\partial\Psi}{\partial\theta_2}\middle|\frac{\partial\Psi}{\partial\theta_1}\right\rangle - \left\langle \frac{\partial\Psi}{\partial\theta_1}\middle|\frac{\partial\Psi}{\partial\theta_2}\right\rangle\right)$. For each GSM of 1/2-FQHE phase with $N_s = 24,\ 36,\ 40$, the two states are found to evolve into each other with level crossings when tuning the boundary phases [Fig. 3(a)]. While for $N_s = 32$, with both states of the GSM in the $(0, 0)$ sector, each state evolves into itself when tuning the boundary phases, and avoided level crossings appear instead [Fig. 3(b)] due to nonzero coupling between same momentum states. The GSM in the FQHE phase also has rather smooth Berry curvature [Fig. 3(c)] and shares a total Chern number $C = 1$.

SF stiffness and structure factors.—The 1/2 FQHE phase on the honeycomb lattice is also distinguished from the other phases by the featureless intra-sublattice (AA) structure factor $S^{\mathrm{AA}}(\mathbf{q})$ [Fig. 4(a)]. The solid phase at a larger V_2 is characterized by a ridge with $q_1 + q_2 = 2\pi$ in the inter-sublattice (AB) structure factor $S^{\mathrm{AB}}(\mathbf{q})$ [Fig. 4 (c)] and an almost vanishing SF stiffness ρ_{SF} [Fig. 4(e)]. The SF phase at a smaller V_2 has the finite ρ_{SF} [Fig. 4(e)] while with a weaker ridge in $S^{\mathrm{AB}}(\mathbf{q})$ [Fig. 4 (b)]. At a fixed $V_1 = 4.0$ while tuning V_2, a transition from the FQHE to the SF phase occurs with the level crossing of E_2 and E_3 around $V_2 = 1.0$ [Fig. 4(d)]; and a transition from the SF phase to the solid phase near

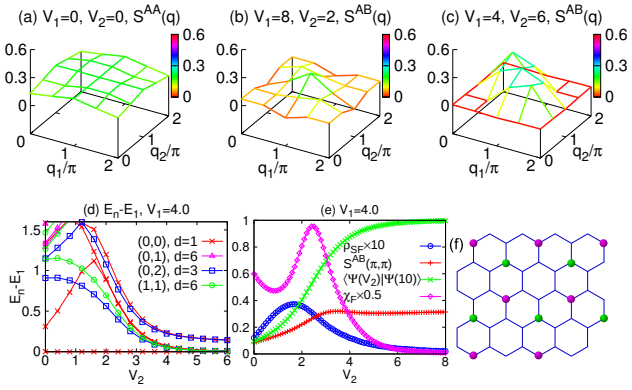

FIG. 4: (color online). 32-site honeycomb lattice at $\nu = 1/2$. (a) $S^{\rm AA}(\mathbf{q})$ of the FQHE phase; (b) $S^{\rm AB}(\mathbf{q})$ of the SF phase; (c) $S^{\rm AB}(\mathbf{q})$ of the solid phase. (d) Excited energy $E_n - E_1$ in various sectors (with d-fold degeneracy) versus V_2 at $V_1 = 4.0$. (e) $\rho_{\rm SF}$, $S^{\rm AB}(\pi,\pi)$, GS overlap $|\langle\Psi(V_2)|\Psi(10)\rangle|$, and fidelity susceptibility $\chi_{\rm F}$ versus V_2, at a fixed $V_1 = 4.0$. (f) Illustration of boson occupancy in the solid phase.

$V_2 = 2.5$ is indicated by a peak of the GS fidelity susceptibility [20] in Fig. 4(e), where $\chi_{\rm F} = 2[1 - |\langle\Psi(V_2)|\Psi(V_2+\delta)\rangle|]/\delta^2$.

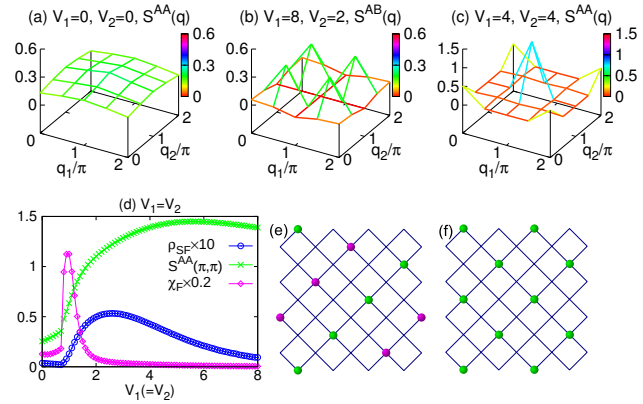

FIG. 5: (color online). 32-site checkerboard lattice at $\nu = 1/2$. (a) $S^{\rm AA}(\mathbf{q})$ of the FQHE phase. (b) $S^{\rm AB}(\mathbf{q})$ of the SS1 phase; (c) $S^{\rm AA}(\mathbf{q})$ of the SS2 phase. (d) $\rho_{\rm SF}$, $S^{\rm AA}(\pi,\pi)$, and $\chi_{\rm F}$ versus V_1 along the $V_1 = V_2$ line. (e)-(f) Illustration of boson occupancy in the SS1 and SS2 phases, respectively.

Similarly, the 1/2 FQHE phase on the checkerboard lattice also differs from the other phases by featureless $S(\mathbf{q})$ [Fig. 5(a)]. While both SS1 and SS2 phases are characterized by either the $\mathbf{q} = (\pi/2, \pi/2)$ peak of $S^{\rm AB}(\mathbf{q})$ [Fig. 5(b)] or the $\mathbf{q} = (\pi,\pi)$ peak of $S^{\rm AA}(\mathbf{q})$ [Fig. 5(c)]. Along the $V_1 = V_2$ line while $V_1 (= V_2)$ being tuned, a transition can be inferred from the FQHE phase to the SS2 phase around $V_1 (= V_2) = 1.0$ by a sharp peak in the GS

fidelity susceptibility [Fig. 5(d)]. We emphasize that the firm establishment of the supersolid and solid phases needs scaling of both $\rho_{\rm SF}$ and $S(\mathbf{q})$ for systems with larger sizes, e.g. $2\times6\times6$ and $2\times8\times8$, which are compatible with the ordering patterns [Figs. 4(f), 5(e), 5(f)] but are far beyond the capability of the present ED method.

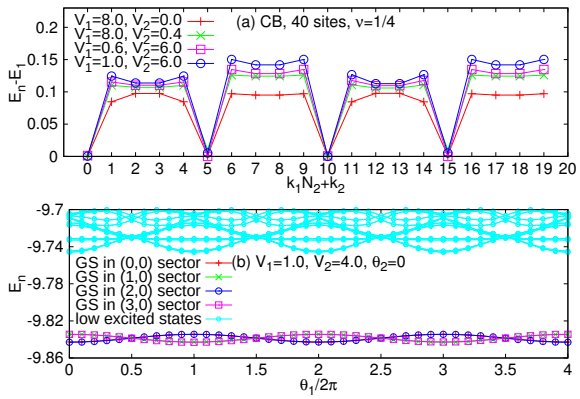

FIG. 6: (color online). The 1/4-FQHE of the 40-site checkerboard model: (a) spectrum gaps $E_n - E_1$ versus $k_1N_2 + k_2$; (b) low energy spectra versus θ_1 at a fixed $\theta_2 = 0$.

The $\nu = 1/4$ FQHE.—We searched for the $\nu = 1/4$ FQHE for both lattice models with the system sizes of $N_s = 24$, 32, 40 and 48. In contrast to the $\nu = 1/2$ case, the onset of the 1/4-FQHE needs finite values of either V_1 or V_2. Examples of the 40-site checkerboard system are chosen to demonstrate the basic properties of the 1/4-FQHE. For each set of V_1 and V_2 in Fig. 6(a), there is clearly a GSM with four states. For each GSM, the four states evolve into each other when tuning the boundary phases [Fig. 6(b)], and all the four states share a total Chern number 1. These are concrete evidences of the 1/4-FQHE in some parameter regions, however, these regions depend on the lattice sizes more sensitively than those of the 1/2-FQHE. We conjecture that a finite NNNN repulsion V_3 may be necessary to get a large and stable parameter space of the 1/4-FQHE, which will be addressed in a future work.

Summary and discussion.—We consider hard-core bosons in two representative TFB models with NN and NNN repulsions. We find convincing numerical evidences of both the 1/2 and the 1/4 bosonic FQHE phases which are characterized by distinctive finite spectrum gap; quasi-degenerate states in a GSM which can evolve into each other upon varying boundary phases; smooth Berry curvature and topologically invariant unit total Chern number for the GSM. For both lattices, the 1/2-FQHE phase is found to occupy a significant

space of phase diagrams, in addition to other conventional ordered phases. Interestingly, such a 1/2-FQHE is very stable (large spectrum gap) for hard-core bosons even without additional interactions ($V_1 = V_2 = 0$), which makes it easier to be realized by cold atoms in optical lattices.

Further understanding of such FQHE in TFBs might involve some recent new ideas. It has been very recently proposed that there is a possible generic FQHE wave-function construction based on localized Wannier basis [25], and the universal quasi-hole counting based upon the generalized Pauli principle [26]. However, a direct comparison of the numerical wave function and model wave functions constructed from the Wannier basis is still absent. From a different point of view, a direct calculation of the topological term in the Feynman path-integral approach may be essential for revealing the underlying cyclotron braid picture and its relation to fractionalization [27].

This work is supported by DOE Office of Basic Energy Sciences under grant DE-FG02-06ER46305 (DNS). We also acknowledge the NSFC of China grant No. 10904130 (YFW), the US NSF grant No. NSFPHY05-51164 (ZCG), and the State Key Program for Basic Researches of China grants No. 2006CB921802 and No. 2009CB929504 (CDG).

[1] N. R. Cooper, Advances in Physics **57**, 539 (2008).

[2] A. S. Sørensen, E. Demler, and M. D. Lukin, Phys. Rev. Lett. **94**, 086803 (2005).

[3] R. N. Palmer and D. Jaksch, Phys. Rev. Lett. **96**, 180407 (2006).

[4] F. D. M. Haldane, Phys. Rev. Lett. **61**, 2015 (1988).

[5] V. M. Yakovenko, Phys. Rev. Lett., **65**, 251 (1990).

[6] K. Ohgushi, S. Murakami, and N. Nagaosa, Phys. Rev. B **62**, R6065 (2000).

[7] D. J. Thouless, M. Kohmoto, M. P. Nightingale, and M. den Nijs, Phys. Rev. Lett. **49**, 405 (1982).

[8] Q. Niu, D. J. Thouless, and Y. S. Wu, Phys. Rev. B **31**, 3372 (1985).

[9] E. Tang, J. W. Mei, and X. G. Wen, Phys. Rev. Lett. **106**, 236802 (2011).

[10] T. Neupert, L. Santos, C. Chamon, and C. Mudry, Phys. Rev. Lett. **106**, 236804 (2011).

[11] K. Sun, Z. C. Gu, H. Katsura, and S. Das Sarma, Phys. Rev. Lett. **106**, 236803 (2011).

[12] C. Wu, D. Bergman, L. Balents, and S. Das Sarma, Phys. Rev. Lett. **99**, 070401 (2007).

[13] D. N. Sheng, Z. C. Gu, K. Sun, and L. Sheng, Nature Commun. **2**, 389 (2011).

[14] C. Wu, Phys. Rev. Lett. **101**, 186807 (2008); M. Zhang, H. H. Hung, C. Zhang, and C. Wu, Phys. Rev. A **83**, 023615 (2011).

[15] L. B. Shao, S. L. Zhu, L. Sheng, D. Y. Xing, and Z. D. Wang, Phys. Rev. Lett. **101**, 246810 (2008).

[16] T. D. Stanescu, V. Galitski, J. Y. Vaishnav, C. W. Clark, and S. Das Sarma, Phys. Rev. A **79**, 053639 (2009); T. D. Stanescu, V. Galitski, and S. Das Sarma, Phys. Rev. A **82**, 013608 (2010).

[17] J. W. Mei, E. Tang, and X. G. Wen, arXiv:1102.2406.

[18] V. Kalmeyer and R. B. Laughlin, Phys. Rev. Lett. **59**, 2095 (1987); X. G. Wen, F. Wilczek, and A. Zee, Phys. Rev. B **39**, 11413 (1989).

[19] D. N. Sheng, X. Wan, E. H. Rezayi, K. Yang, R. N. Bhatt, and F. D. M. Haldane, Phys. Rev. Lett. **90**, 256802 (2003).

[20] S. J. Gu, Int. J. Mod. Phys. B **24**, 4371 (2010).

[21] C. N. Varney, K. Sun, M. Rigol, and V. Galitski, Phys. Rev. B **82**, 115125 (2010); C. N. Varney, K. Sun, V. Galitski, and M. Rigol, Phys. Rev. Lett. **107**, 077201 (2011). In which the bosonic Haldane model with integer filling was studied.

[22] F. Li, L. Sheng and D. Y. Xing, Europhys. Lett. **84**, 60004 (2008).

[23] K. Sun, H. Yao, E. Fradkin, and S. A. Kivelson, Phys. Rev. Lett. **103**, 046811 (2009).

[24] P. W. Leung and P. E. Oppenheimer, Comput. Phys. **6**, 603 (1992); H. Q. Lin and J. E. Gubernatis, Comput. Phys. **7**, 400 (1993).

[25] X. L. Qi, arXiv:1105.4298.

[26] N. Regnault and B. A. Bernevig, arXiv:1105.4867.

[27] J. Jacak and L. Jacak, Europhys. Lett. **92**, 60002 (2010).